

# Stiffness of the human foot and evolution of the transverse arch

<https://doi.org/10.1038/s41586-020-2053-y>

Received: 29 March 2018

Accepted: 23 January 2020

Published online: 26 February 2020

 Check for updates

Madhusudhan Venkadesan<sup>1✉</sup>, Ali Yawar<sup>1</sup>, Carolyn M. Eng<sup>1,10</sup>, Marcelo A. Dias<sup>2,3,4,10</sup>, Dhiraj K. Singh<sup>5,9</sup>, Steven M. Tommasini<sup>6</sup>, Andrew H. Haims<sup>6,7</sup>, Mahesh M. Bandi<sup>5✉</sup> & Shreyas Mandre<sup>8✉</sup>

The stiff human foot enables an efficient push-off when walking or running, and was critical for the evolution of bipedalism<sup>1–6</sup>. The uniquely arched morphology of the human midfoot is thought to stiffen it<sup>5–9</sup>, whereas other primates have flat feet that bend severely in the midfoot<sup>7,10,11</sup>. However, the relationship between midfoot geometry and stiffness remains debated in foot biomechanics<sup>12,13</sup>, podiatry<sup>14,15</sup> and palaeontology<sup>4–6</sup>. These debates centre on the medial longitudinal arch<sup>5,6</sup> and have not considered whether stiffness is affected by the second, transverse tarsal arch of the human foot<sup>16</sup>. Here we show that the transverse tarsal arch, acting through the inter-metatarsal tissues, is responsible for more than 40% of the longitudinal stiffness of the foot. The underlying principle resembles a floppy currency note that stiffens considerably when it curls transversally. We derive a dimensionless curvature parameter that governs the stiffness contribution of the transverse tarsal arch, demonstrate its predictive power using mechanical models of the foot and find its skeletal correlate in hominin feet. In the foot, the material properties of the inter-metatarsal tissues and the mobility of the metatarsals may additionally influence the longitudinal stiffness of the foot and thus the curvature–stiffness relationship of the transverse tarsal arch. By analysing fossils, we track the evolution of the curvature parameter among extinct hominins and show that a human-like transverse arch was a key step in the evolution of human bipedalism that predates the genus *Homo* by at least 1.5 million years. This renewed understanding of the foot may improve the clinical treatment of flatfoot disorders, the design of robotic feet and the study of foot function in locomotion.

When walking and running, people use the ball of the foot to apply forces that exceed bodyweight<sup>17</sup>. Because of these forces, the midfoot experiences large sagittal-plane torques that bend the foot. A stiff midfoot reduces the loss of propulsive work due to foot deformation and helps to efficiently utilize the mechanical power generated by the ankle during push-off<sup>2–4</sup>.

The unique arch shape of the human midfoot is thought to underlie the higher stiffness of human feet compared to other primate feet<sup>5,6,9,18</sup> (Extended Data Table 1). However, stiffness is not a static quantity and muscle activity can modulate midfoot stiffness in both humans and apes<sup>13,19,20</sup>. The static stiffness due to the passive structures of the foot forms the baseline around which muscles with similar mechanical action as the passive tissues are likely to modulate stiffness. Therefore, understanding the morphological features underpinning the static stiffness is crucial for both static and dynamic conditions (Supplementary Information 1.1–1.3).

The human midfoot has two pronounced arches: the extensively studied medial longitudinal arch (MLA)<sup>5,6,20</sup> and the less-studied

transverse tarsal arch (TTA) (Fig. 1a). The MLA stiffens the midfoot in part through a bow-string arrangement with the stiff longitudinal fibres of the plantar fascia<sup>7,9</sup> and a windlass-like mechanism due to toe dorsiflexion just before push-off<sup>8,21</sup>. In addition to the plantar fascia, the longitudinally oriented long plantar, short plantar and calcaneonavicular ligaments are essential for the static midfoot stiffness in humans and other primates<sup>9,18</sup>. However, in contrast to the plantar fascia, the contribution of these ligaments does not depend on the height of the MLA, as shown by their nearly equal relative contributions in both arched human feet<sup>9</sup> and flat monkey feet<sup>18</sup> (Extended Data Table 1 and Supplementary Information 1.4).

The relationship between the height or curvature of the MLA and midfoot stiffness remains controversial<sup>5,20</sup>. Some people have no difficulty walking with a heel-to-toe style despite having little to no MLA<sup>12</sup>. Conflicting evidence also emerges in foot disabilities<sup>11,22</sup> and surgical reconstruction of the MLA<sup>15</sup> when correlating MLA height with foot flexibility, and casts further doubt on the relationship between the

<sup>1</sup>Department of Mechanical Engineering and Materials Science, Yale University, New Haven, CT, USA. <sup>2</sup>School of Science, Aalto University, Espoo, Finland. <sup>3</sup>Nordic Institute for Theoretical Physics (NORDITA), Stockholm, Sweden. <sup>4</sup>Department of Engineering, Aarhus University, Aarhus, Denmark. <sup>5</sup>Nonlinear and Non-equilibrium Physics Unit, OIST Graduate University, Onna, Japan. <sup>6</sup>Department of Orthopaedics and Rehabilitation, Yale University, New Haven, CT, USA. <sup>7</sup>Department of Radiology and Biomedical Imaging, Yale University, New Haven, CT, USA.

<sup>8</sup>Mathematics Institute, University of Warwick, Coventry, UK. <sup>9</sup>Present address: Engineering Mechanics Unit, Jawaharlal Nehru Centre for Advanced Scientific Research, Bangalore, India.

<sup>10</sup>These authors contributed equally: Carolyn M. Eng, Marcelo A. Dias. ✉e-mail: m.venkadesan@yale.edu; bandi@oist.jp; shreyas.mandre@warwick.ac.uk

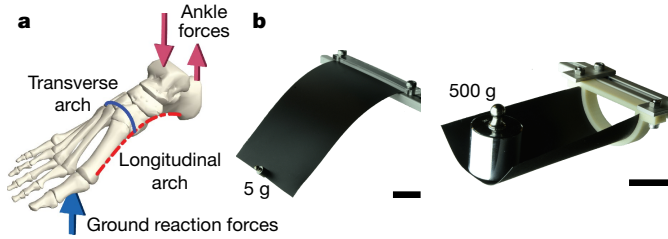


**Fig. 1 | Transverse curvature and stiffness.** **a**, The human foot has two distinct arches in the midfoot, the MLA and the TTA. Further anatomical details are shown in Extended Data Fig. 1. The typical loading pattern during push-off in walking and running is shown here. **b**, A thin and floppy sheet of paper becomes considerably stiffer because of transversal curvature. The TTA may have a similar role in feet. Scale bars, 5 cm.

MLA and midfoot stiffness. Furthermore, there are also debates over when a stiff midfoot arose in human evolution<sup>5,6</sup>, including what kind of foot made the 3.66-million-year-old partly human-like footprints at Laetoli<sup>23,24</sup>.

These debates regarding the arch morphology and stiffness centre around the MLA, the plantar fascia and other longitudinally oriented ligaments and muscles, and do not consider the role of the TTA (Supplementary Information 1.4). Even the definition of flatfoot relies mostly on the height of the MLA<sup>12,22</sup>. However, the TTA may affect midfoot stiffness, similar to how even slightly curling a thin sheet of paper in the transverse direction stiffens the paper longitudinally (Fig. 1b). To investigate whether the TTA functions in this manner, we performed three-point bending tests on arched continuum shells, mechanical mimics of the midfoot and human cadaveric feet.

We investigated the relationship between curvature and stiffness by modelling the TTA as a curved elastic shell in computer simulations and physical experiments (Fig. 2a). We found that shells with greater transverse curvature were stiffer in longitudinal bending (Fig. 2b). However, the stiffness also depended on the thickness  $t$ , length  $L$ , width  $w$ , Young’s modulus and Poisson’s ratio of the material. To isolate the contribution of the transverse arch to midfoot stiffness, we used scaling analysis to derive dimensionless variables for stiffness and curvature that are normalized for material property and size differences (Supplementary Information 2). The normalized stiffness  $\hat{K}$  is the ratio of the stiffness of the curved shell to that of a flat plate that is identical except for the curvature. The normalized curvature  $\hat{c}$  encapsulates the mechanical coupling between bending out-of-plane and stretching in-plane that is induced by the transverse curvature  $c$ , and is given by

$$\hat{c} = \frac{cL^2}{t} \quad (1)$$

Collapse of the normalized data onto a master curve shows that  $\hat{c}$  is the chief explanatory variable for  $\hat{K}$  (Fig. 2b). There is a transition between two regimes around  $\hat{c}_{tr} = 10$ . Stiffness  $\hat{K}$  increases nonlinearly with curvature when  $\hat{c} > \hat{c}_{tr}$  but is mostly insensitive to curvature when  $\hat{c} < \hat{c}_{tr}$ . Increasing the longitudinal curvature has no effect on stiffness (Fig. 2b), because these shells lack any analogue of the plantar fascia. Transverse curvature stiffens the shell because out-of-plane longitudinal bending induces in-plane stretching of the material of the shell close to the load application point (Extended Data Fig. 2 and Supplementary Information 2). Therefore, the transverse curvature has the effect of amplifying the intrinsic stiffness of a flat plate, whereas the longitudinal curvature has no similar effect.

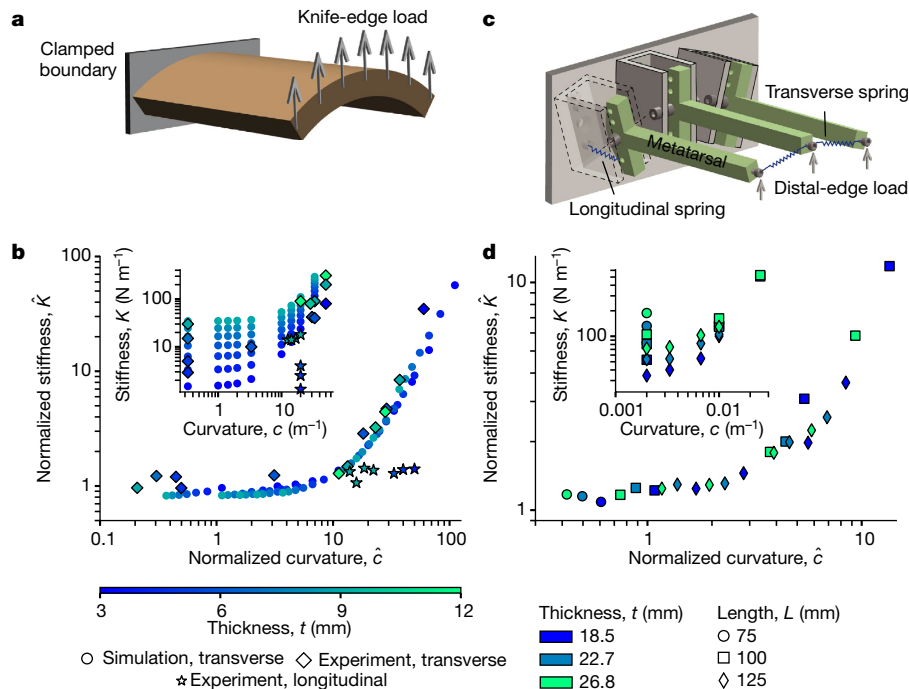


**Fig. 2 | Curvature-induced stiffness in mechanical models of hominin feet.**

**a**, Continuum elastic shells with curvature were subjected to a distributed vertical load at one end and clamped at the other. **b**, The shell data using normalized stiffness ( $\hat{K}$ ) and normalized curvature ( $\hat{c}$ ). The shells were transversally (diamonds) or longitudinally (stars) curved. Inset, stiffness ( $K$ ) versus curvature ( $c$ ) for continuum shells of various thicknesses ( $t$ ) (blue shading) in experiments (diamonds and stars) and simulations (circles). **c**, The discrete foot mimics consisted of three metatarsals arranged in a transverse

arch and loaded at the distal end. Longitudinal springs at the hinged base mimic the longitudinal ligaments in feet. Transversal inter-metatarsal springs at the distal end mimic transverse elastic tissues. **d**, The foot-mimic data using normalized stiffness ( $\hat{K}$ ) and normalized curvature ( $\hat{c}$ ). Inset, stiffness ( $K$ ) versus transverse curvature ( $c$ ) for mimics of various lengths ( $L$ ) and thicknesses ( $t$ ). Detailed views of the continuum and discrete experiments are in Extended Data Figs. 3 and 4, respectively.

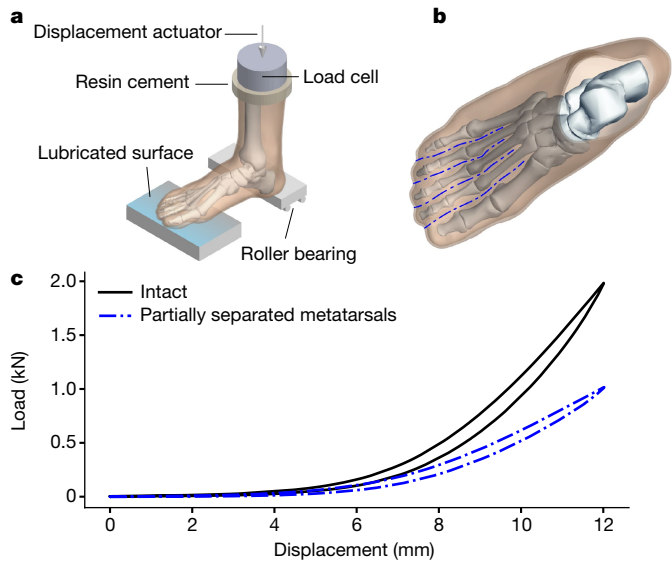


**Fig. 3 | Three-point bending test on a cadaveric human foot.** **a**, Fresh-frozen cadaveric feet ( $n = 2$ ) were thawed and mounted in a materials-testing machine using an attachment at the transected shank. The distal end of the heel rested on a sliding platform with low-friction roller bearings to enable changes in foot length. The ball of the foot and the toes rested on a lubricated surface. The transected shank was displaced downward and the reaction force was measured. Tests were performed on intact feet and those with transversal cuts. **b**, The transversal cuts between the toes and metatarsals (dashed blue lines) were no deeper than the plantar plane of the metatarsal shafts. **c**, Displacement versus force traces for an intact foot (solid black line) and a foot with partially separated metatarsals (dashed blue line) foot. Some stress relaxation was observed during the initial few cycles of testing and the last cycle was used for analyses.

We performed three-point bending tests on discrete mechanical mimics of the foot with a TTA and found similar results to the continuum shells (Fig. 2c, d). The mimics, which consisted of three metatarsals

with hinges towards the midfoot, are of length  $L$ , thickness  $t$  and transverse curvature  $c$  (Methods and Supplementary Information 4). The longitudinal springs at the hinges mimic the longitudinal midfoot ligaments that contribute to midfoot stiffness whether arched or not (Supplementary Information 1.4). The distally located transverse springs mimic inter-metatarsal tissues that influence the predicted bending–stretching coupling due to the transverse curvature. We find that the normalized curvature  $\hat{c}$  accurately predicts the normalized stiffness  $\hat{K}$  for discrete foot-like structures, as for continuum shells (Fig. 2d; Methods, equation (2)). The transition in stiffness from nearly curvature-insensitive to a nonlinear increase occurs around  $\hat{c}_{tr} = 3$  for the mimics. Although this value is different from continuum shells, bending–stretching coupling is the common mechanism for curvature-induced stiffness and  $\hat{c}$  emerges as the chief explanatory variable.

The role of the TTA in human feet could be found by measuring the decrease in stiffness upon flattening the TTA; however, altering the TTA would also affect other elements, such as the MLA. We therefore designed a method that emulates flattening the TTA without altering the skeletal structure. The main idea is that the transverse curvature induces stiffness by coupling longitudinal bending with stretching of the inter-metatarsal tissues, as shown by the analyses of the continuum shells and mechanical mimics, and as is also evident in mathematical models of rayed fish fins with transverse curvature<sup>25</sup>. Therefore, cutting the inter-metatarsal tissues should disrupt the stiffening mechanism and emulate flattening the arch without altering the skeletal structure. We tested this idea in the foot mimics by comparing the stiffness of transversally curved mimics that lack the inter-metatarsal springs with flat mimics that had all springs intact. Both had the same stiffness ( $R^2 = 0.98$ , slope = 1.05, intercept = 0) (Extended Data Fig. 5), showing that cutting the transverse springs disengages the mechanism through which transverse curvature increases the longitudinal stiffness.

To determine the contribution of the TTA to stiffness in human feet, we performed three-point bending tests on two human cadaveric feet (Fig. 3a, Methods and Supplementary Information 5.2) and assessed the effect of selectively cutting the transverse tissues between the metatarsals (T<sup>-</sup> condition) (Fig. 3b). To carefully preserve longitudinal tissues, we cut only the transverse metatarsal ligaments, the skin

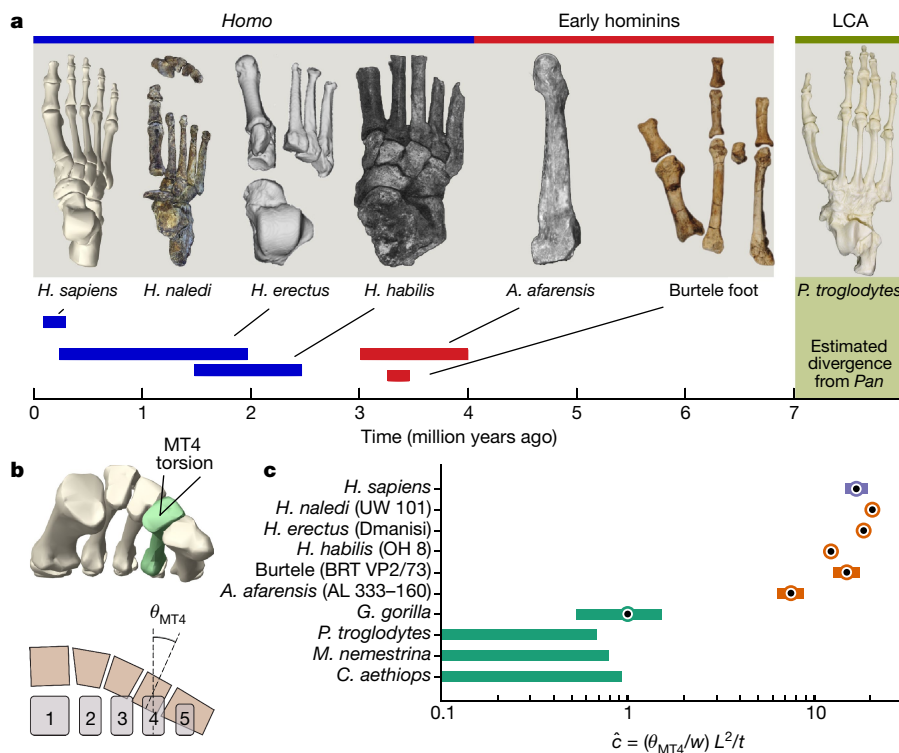


**Fig. 4 | Transverse curvature of extant and extinct feet.** **a**, Representative images of feet used in our analyses and their respective estimated survival dates: *H. naledi*<sup>26</sup>, *H. erectus*<sup>28</sup>, *H. habilis*<sup>27</sup>, *A. afarensis*<sup>30</sup> and Burtele<sup>29</sup>. *Pan troglodytes* represents the last common ancestor (LCA) of humans and chimpanzees. **b**, Schematics showing the skeletal view of the TTA and the torsion of the fourth metatarsal induced by the mediolateral packing of the tarso-metatarsal bones. **c**, Median (dot with circle) and the middle 50th percentile (shaded bar) of the normalized curvature ( $\hat{c}$ ) are shown on a logarithmic scale. Extended Data Tables 2, 3 summarize the morphometric data used to estimate  $\hat{c}$ . Monte Carlo simulations generated the statistics for all of the samples except for the genus *Homo*. The number of independent samples used to derive the statistics: *Homo sapiens*,  $n = 12$ ; *H. naledi*,  $n = 1$ ; *H. erectus*,  $n = 1$ ; *H. habilis*,  $n = 1$ ; Burtele,  $n = 1$ ; *A. afarensis*,  $n = 1$ ; *Gorilla gorilla*,  $n = 59$ ; *P. troglodytes*,  $n = 106$ ; *Macaca nemestrina*,  $n = 44$ ; *Chlorocebus aethiops*,  $n = 56$ .

between the toes and the inter-metatarsal tissues below the dorsal surface of the foot. The mechanical work to deform the foot is a measure of stiffness (Supplementary Information 5.3) and cutting these transverse tissues decreased stiffness by 44% and 54% for the two feet (Fig. 3b and Extended Data Table 1). Each foot serves as its own control, thereby quantifying the contribution of the TTA as the normalized stiffness  $\hat{K} = K_{\text{intact}}/K_{\text{T-}}$ . We found  $\hat{K} = 1.77$  and  $\hat{K} = 2.18$  for the feet for which  $\hat{c} = 15.4$  and  $\hat{c} = 16.0$ , respectively (Fig. 4b; Methods, equation (5)).

The cadaveric experiments show that the inter-metatarsal tissues contribute substantially to foot stiffness, and more than the previously described contribution of the MLA and plantar fascia of 23% (Extended Data Table 1 and Supplementary Information 1.4). In addition to curvature of the TTA, the stiffness and slack of the inter-metatarsal tissues as well as the mobility of the metatarsals may ultimately combine to tune the longitudinal stiffness of the foot and thus influence the curvature–stiffness relationship of the TTA. Therefore, additional data are needed to find the precise curvature–stiffness relationship in human feet. Nevertheless, the mechanistic understanding of transversally curved structures suggests that the inter-metatarsal tissues affect the longitudinal bending stiffness of the foot because the human TTA, with  $\hat{c} \approx 15$ , is sufficiently arched to couple longitudinal bending and transverse stretching.

We use  $\hat{c}$  to compare and track the evolution of the TTA among hominins (Fig. 4 and Supplementary Information 5). At one extreme are the feet of the vervet monkey, macaque, chimpanzee and gorilla, which have  $\hat{c} < 3$  and are substantially flatter than those of humans, which have  $\hat{c} > 10$ . At the other extreme are species in the genus *Homo*, including *Homo naledi*<sup>26</sup>, *Homo habilis*<sup>27</sup> and *Homo erectus*<sup>28</sup> that possess a pronounced TTA with a human-like  $\hat{c} \approx 15$ . The estimated  $\hat{c}$  of the approximately 3.4-million-year-old Burtele foot (from an unidentified species) falls within the normal variation of humans despite having an abducted hallux<sup>29</sup>. By contrast, the estimated  $\hat{c}$  of the approximately 3.2-million-year-old *Australopithecus afarensis* (AL-333) falls below the human range, despite a human-like torsion of the fourth metatarsal<sup>30</sup>.

Additional data are needed, especially from earlier hominins such as *Ardipithecus*; however, the available evidence suggests that there were several stages in the evolution of the arch of the human foot<sup>5,6</sup>. First, apes such as chimpanzees and presumably the last common ancestor of apes and hominins lack both a MLA and a TTA, and thus are able to stiffen the midfoot only partially using muscles<sup>5</sup>. By 3.4 million years ago, and possibly earlier, a human-like TTA had evolved that may have increased midfoot stiffness during propulsion in the Burtele hominin (Supplementary Information 5.4). Compared with humans, the TTA was apparently less developed in *A. afarensis*, which also lacked a fully developed MLA<sup>30</sup>—consistent with analyses of the 3.66-million-year-old Laetoli G footprints that are thought to have been made by *A. afarensis*<sup>24,31</sup>. Finally, in the genus *Homo* we see a full MLA and TTA, enabling both effective walking and running. These inferences need to be tested with additional fossils incorporating not only analyses of the MLA but also the TTA.

Our findings show a previously undescribed and substantial role for the TTA in midfoot stiffness. Traditional thinking in biomechanics, human evolution and clinical practice, with an emphasis on the sagittal plane and the MLA, should thus be expanded to incorporate the TTA and the transverse axis that is orthogonal to the sagittal plane.

## Online content

Any methods, additional references, Nature Research reporting summaries, source data, extended data, supplementary information,

acknowledgements, peer review information; details of author contributions and competing interests; and statements of data and code availability are available at <https://doi.org/10.1038/s41586-020-2053-y>.

- Susman, R. L. Evolution of the human foot: evidence from Plio-Pleistocene hominids. *Foot Ankle* **3**, 365–376 (1983).
- Bramble, D. M. & Lieberman, D. E. Endurance running and the evolution of *Homo*. *Nature* **432**, 345–352 (2004).
- Takahashi, K. Z., Gross, M. T., van Werkhoven, H., Piazza, S. J. & Sawicki, G. S. Adding stiffness to the foot modulates soleus force-velocity behaviour during human walking. *Sci. Rep.* **6**, 29870 (2016).
- Pontzer, H. Economy and endurance in human evolution. *Curr. Biol.* **27**, R613–R621 (2017).
- Holowka, N. B. & Lieberman, D. E. Rethinking the evolution of the human foot: insights from experimental research. *J. Exp. Biol.* **221**, jeb174425 (2018).
- DeSilva, J., McNutt, E., Benoit, J. & Zipfel, B. One small step: a review of Plio-Pleistocene hominin foot evolution. *Am. J. Phys. Anthropol.* **168**, 63–140 (2019).
- Morton, D. J. Evolution of the longitudinal arch of the human foot. *J. Bone Joint Surg.* **6**, 56–90 (1924).
- Hicks, J. H. The mechanics of the foot: II. The plantar aponeurosis and the arch. *J. Anat.* **88**, 25–30 (1954).
- Ker, R. F., Bennett, M. B., Bibby, S. R., Kester, R. C. & Alexander, R. M. The spring in the arch of the human foot. *Nature* **325**, 147–149 (1987).
- D'Août, K., Aerts, P., De Clercq, D., De Meester, K. & Van Elsacker, L. Segment and joint angles of hind limb during bipedal and quadrupedal walking of the bonobo (*Pan paniscus*). *Am. J. Phys. Anthropol.* **119**, 37–51 (2002).
- Bates, K. T. et al. The evolution of compliance in the human lateral mid-foot. *Proc. R. Soc. B* **280**, 20131818 (2013).
- DeSilva, J. M. et al. Midtarsal break variation in modern humans: functional causes, skeletal correlates, and paleontological implications. *Am. J. Phys. Anthropol.* **156**, 543–552 (2015).
- Holowka, N. B., O'Neill, M. C., Thompson, N. E. & Demes, B. Chimpanzee and human midfoot motion during bipedal walking and the evolution of the longitudinal arch of the foot. *J. Hum. Evol.* **104**, 23–31 (2017).
- MacKenzie, A. J., Rome, K. & Evans, A. M. The efficacy of nonsurgical interventions for pediatric flexible flat foot: a critical review. *J. Pediatr. Orthop.* **32**, 830–834 (2012).
- Baxter, J. R. et al. Reconstruction of the medial talonavicular joint in simulated flatfoot deformity. *Foot Ankle Int.* **36**, 424–429 (2015).
- Morton, D. J. Evolution of the human foot II. *Am. J. Phys. Anthropol.* **7**, 1–52 (1924).
- Hayafune, N., Hayafune, Y. & Jacob, H. Pressure and force distribution characteristics under the normal foot during the push-off phase in gait. *Foot* **9**, 88–92 (1999).
- Bennett, M. B., Ker, R. F. & Alexander, R. M. Elastic strain energy storage in the feet of running monkeys. *J. Zool.* **217**, 469–475 (1989).
- Farris, D. J., Kelly, L. A., Cresswell, A. G. & Lichtwark, G. A. The functional importance of human foot muscles for bipedal locomotion. *Proc. Natl Acad. Sci. USA* **116**, 1645–1650 (2019).
- Heard-Booth, A. N. *Morphological and Functional Correlates of Variation in The Human Longitudinal Arch*. PhD thesis, Univ. Texas, Austin (2017).
- Griffin, N. L., Miller, C. E., Schmitt, D. & D'Août, K. Understanding the evolution of the windlass mechanism of the human foot from comparative anatomy: insights, obstacles, and future directions. *Am. J. Phys. Anthropol.* **156**, 1–10 (2015).
- Williams, D. S. & McClay, I. S. Measurements used to characterize the foot and the medial longitudinal arch: reliability and validity. *Phys. Ther.* **80**, 864–871 (2000).
- Leakey, M. D. & Hay, R. L. Pliocene footprints in the Laetoli Beds at Laetoli, northern Tanzania. *Nature* **278**, 317–323 (1979).
- Crompton, R. H. et al. Human-like external function of the foot, and fully upright gait, confirmed in the 3.66 million year old Laetoli hominin footprints by topographic statistics, experimental footprint-formation and computer simulation. *J. R. Soc. Interface* **9**, 707–719 (2012).
- Nguyen, K., Yu, N., Bandi, M. M., Venkadesan, M. & Mandre, S. Curvature-induced stiffening of a fish fin. *J. R. Soc. Interface* **14**, 20170247 (2017).
- Harcourt-Smith, W. E. H. et al. The foot of *Homo naledi*. *Nat. Commun.* **6**, 8432 (2015).
- Day, M. H. & Napier, J. R. Fossil foot bones. *Nature* **201**, 969–970 (1964).
- Pontzer, H. et al. Locomotor anatomy and biomechanics of the Dmanisi hominins. *J. Hum. Evol.* **58**, 492–504 (2010).
- Haile-Selassie, Y. et al. A new hominin foot from Ethiopia shows multiple Pliocene bipedal adaptations. *Nature* **483**, 565–569 (2012).
- Ward, C. V., Kimbel, W. H. & Johanson, D. C. Complete fourth metatarsal and arches in the foot of *Australopithecus afarensis*. *Science* **331**, 750–753 (2011).
- Raichlen, D. A., Gordon, A. D., Harcourt-Smith, W. E., Foster, A. D. & Haas, W. R. Jr. Laetoli footprints preserve earliest direct evidence of human-like bipedal biomechanics. *PLoS ONE* **5**, e9769 (2010).

**Publisher's note** Springer Nature remains neutral with regard to jurisdictional claims in published maps and institutional affiliations.

© The Author(s), under exclusive licence to Springer Nature Limited 2020

## Methods

### Data reporting

No statistical methods were used to predetermine sample size. The experiments were not randomized and the investigators were not blinded to allocation during experiments and outcome assessment.

### Ethical compliance

The authors have complied with all relevant ethical regulations in conducting the research for this paper.

### Numerical simulations

We simulated the elastic response of arched shells using the Shell interface in the 3D Structural Mechanics module of COMSOL Multiphysics v.5.1 (COMSOL AB). The TTA is represented by the map for the central plane of the shell given by  $\mathbf{S}_T(x, y) = (x, R_T \sin \theta_y, R_T \cos \theta_y)$  in which  $\theta_y = y/R_T$ ,  $x \in [-L/2, L/2]$  and  $y \in [-w/2, w/2]$  (Extended Data Fig. 2). For all the simulations, we set  $L = 0.1$  m and  $w = 0.05$  m. The material was modelled as linearly elastic with Young's modulus  $E = 3.5$  MPa, Poisson's ratio  $\nu = 0.49$  and mass density  $\rho = 965$  kg m<sup>-3</sup>.

The boundary at  $x = -L/2$  is clamped—that is, zero displacements and rotations. The conditions at the other boundary  $x = L/2$  are a uniform shear load  $\mathcal{T}$ , zero bending moment along  $z$  and zero in-plane traction so that the displacements are free (see Extended Data Fig. 2 for orientations of the axes).

We solve this model for a range of thicknesses  $t$ , from 3 mm to 9 mm in steps of 1 mm, and transverse curvature radii  $R_T = 0.03$  m, 0.05 m, 0.07 m, 0.1 m, 0.3 m, 0.5 m, 0.7 m, 1 m and 3 m. For each combination of  $t$  and  $R_T$ , shear  $\mathcal{T}$  ranging from 0 N m<sup>-1</sup> to 1 N m<sup>-1</sup> is applied in increments of 0.1 N m<sup>-1</sup>. The resulting out-of-plane displacement  $\delta z$  is measured (Extended Data Fig. 2b) and plotted against  $\mathcal{T}$ . The slope of these curves extrapolated to  $\mathcal{T} = 0$  yield the stiffness defined as  $k \equiv w\mathcal{T}/\delta z$ .

### Continuum shell experiments

We fabricated and measured the stiffness of shells with an arch in the transverse or longitudinal directions, and compared them against a flat plate. These were all fabricated using polymer moulding techniques with polydimethylsiloxane (PDMS). The mould was fabricated using additive manufacturing (3D printed using ProJet 460Plus, 3D Systems). The printed mould was a few millimetres in thickness, with one side left open. A PDMS silicone elastomer (Sylgard 184, Dow Corning) was used to cast the arch in the mould. Because the volume ratio of the base polymer to the curing agent controls the material bulk modulus for PDMS, the same ratio of five parts base polymer to one part of curing agent by weight was consistently maintained across all fabricated arches (Supplementary Information 3). During an experiment, the fabricated arch was mounted on the experimental rig with help of clamps that were custom-fabricated to exactly match the arch curvature. The clamps were additively manufactured (Stratasys Dimension 1200es) with acrylonitrile butadiene styrene (ABSPlus) thermoplastic material (glass transition temperature, 108 °C). One end of the clamped arch was fixed to a rigid frame and the other end of the clamped arch was pushed upon by a thin edge (knife edge) that was mounted on a force sensor attached to a vertical translation stage (Extended Data Fig. 3a). The forces were measured using a data-acquisition system (LabView, National Instruments) at 2 kHz for a duration of 1 s. The load test was performed under quasi-static loading of the arch sample by providing small displacements (quasi-static steps) of  $5 \times 10^{-5}$  m (50  $\mu$ m) per step for a total of 10 quasi-static steps ( $5 \times 10^{-4}$  m or 500  $\mu$ m). Forces were measured after each quasi-static displacement. The slope of the force–displacement curve is the stiffness  $K$  for the arch sample. Three experimental runs were conducted for each arch and their force–displacement curves were reproducible to within measurement error.

### Foot mimics

We designed, fabricated and performed load–displacement tests on mechanical mimics of the foot that were transversally curved (Fig. 2, Extended Data Fig. 4 and Supplementary Information 4). The mimic consisted of three rigid metatarsals hinged at their bases. Instead of every bone in the foot, the mimics were simplifications that captured the longitudinal bending of the metatarsals and lumped all midfoot mobility into hinges at the proximal base of the metatarsals.

The metatarsals were of length  $L$  and the hinges were arranged in a transverse arch of curvature  $c$  so that the axis of each hinge was at an angle with its neighbour (Fig. 2c and Extended Data Fig. 4a). Each hinge had an extension spring held at a fixed moment arm equal to half the thickness  $t$  and provided torsional stiffness (Extended Data Fig. 4b). An inter-metatarsal transversally oriented spring connected adjacent metatarsals at the distal end and would resist any splaying induced by the transverse arch.

In hominin feet, the distal end of the metatarsals are level on the ground when loaded. Therefore, the presence of a TTA suggests increasing torsion for the lateral metatarsals (Extended Data Fig. 6b, c). The distal end of the metatarsals in the mimics were made to rest on horizontal, low-friction metallic platforms (Extended Data Fig. 4a). The vertically staggered arrangement of the platforms mimics the effect of the distal end of the metatarsals being on the same horizontal level. The platforms were attached to a micrometre-precision translation stage for applying vertical displacements. The base of the hinges were rigidly clamped to a six-axis force sensor (JR3) to measure the reaction forces due to the displacement. Stiffness was estimated as the slope of the force–displacement curve in each trial.

Multiple geometries were tested and the dimensions chosen to approximate the metatarsal lengths and midfoot widths of hominin feet, including chimpanzees and humans. The length  $L$  was varied from 75 to 125 mm (3 values), thickness  $t$  from 18.5 to 26.8 mm (3 values) and curvature from 0 to 0.025 mm<sup>-1</sup> (6 values). The spring constants, measured in an Instron materials testing machine, were 1.76 N mm<sup>-1</sup> and 0.70 N mm<sup>-1</sup> for the longitudinal and transverse springs, respectively. Three trials were performed for each foot and the force–displacement data were reproducible to within measurement error.

The normalized stiffness is  $\hat{K} = K/K_{\text{flat}}$ . For a flat mimic with three metatarsals, each of length  $L$ , thickness  $t$  and having a longitudinally oriented spring at its base of stiffness  $k_m$ , the longitudinal stiffness is given by  $K_{\text{flat}} = 3k_m(t/2)^2/L^2$  (Supplementary Information 4.3). In a general setting, the longitudinal spring stiffness would be proportional to the width  $w$  of the midfoot by virtue of accommodating a greater amount of parallel elastic tissues. Therefore, the longitudinal stiffness is equivalently parameterized by the stiffness per unit width  $k_c = 3k_m/w$ .

Supplementary equation (4.4) for the stiffness of a flat mimic was independently verified using load–displacement tests of eight different flat mimics (Extended Data Fig. 4c and Supplementary Information 4.4). We use this relationship to normalize the measured stiffness of all of the mimics by a single chimpanzee-like flat mimic of length  $L_0 = 75$  mm, thickness  $t_0 = 18.5$  mm and width  $w_0 = 60$  mm, and for which the measured stiffness is  $K_0$ . By definition, the normalized stiffness of the chimpanzee-like flat mimic is  $\hat{K}_0 = 1$ . Therefore, the measured stiffness  $K$  of a mimic with length  $L$ , thickness  $t$  and width  $w$  is normalized according to

$$\hat{K} = \frac{K}{K_0} \left( \frac{L}{L_0} \right)^2 \left( \frac{t_0}{t} \right)^2 \left( \frac{w_0}{w} \right) \quad (2)$$

### Cadaveric feet

We conducted three-point bending tests using a materials testing system (Instron model 8874) on two fresh-frozen cadaveric feet obtained from posthumous female donors (age, 55 and 64 years, body weight,

1,023 N and 596 N). The loading protocol and boundary conditions under the foot were as previously described<sup>9</sup>. The tibia and fibula were transected midshaft and implanted in Bondo Fibreglass Resin (3M) and secured to the displacement-controlled force sensor on the Instron actuator. The ankle was at a neutral angle of 90°. The heel rested on a rigid platform that was mounted on low-friction sliders to permit foot-length changes. The forefoot rested on a highly lubricated surface to permit the foot to naturally deform in all directions when loaded. The contact point on the heel was maintained at the posterior end by placing the heel at the anterior edge of the sliding heel plate so that the heel force mimics the action of the Achilles tendon. The tests were quasi-static with a displacement rate of 0.5 mm s<sup>-1</sup> to 0.6 mm s<sup>-1</sup>.

The displacement  $z_{\text{peak}}$  required to achieve a load of 3× the body weight was measured and then cyclically applied 10–15 times. The last cycle was used for analyses because there was some stress relaxation during the first 6–7 cycles. The area under the curve of the displacement  $z$  versus the force  $F$  is the work  $W$  needed to deform the foot. Following Supplementary equation (5.4),  $W$  yields an effective stiffness of the foot  $K_{\text{eff}}$  given by

$$K_{\text{eff}} = \frac{2}{z_{\text{peak}}^2} \int_0^{z_{\text{peak}}} F dz \quad (3)$$

The same measurements were repeated after bisecting the distal transverse metatarsal ligaments, the skin between the toes, and the muscles and fascia connecting the metatarsals. The inter-metatarsal tissues were transected from the dorsal surface of the foot and the cuts extended no deeper than the plantar plane of the metatarsal shafts. Therefore, none of the branches of the plantar fascia or other midfoot ligaments was affected.

Because the applied displacement was the same for the intact feet and those with bisected inter-metatarsal tissues, the ratio of work is equal to the ratio of the effective stiffness (Supplementary equation (5.5)).

## Monte Carlo simulations

Anatomical variability in the size of feet (Extended Data Table 2) is incorporated using Monte Carlo simulations to generate statistics for normalized curvature (Fig. 4). The histograms generated from the Monte Carlo simulations are mostly non-Gaussian. Therefore, the median and quartiles are reported in addition to the mean and s.d. We used 1 million random combinations of the anatomical dimensions, in which each dimension was drawn from an independent Gaussian distribution with mean and s.d. values according to Extended Data Table 2, 3. Increasing the size of the Monte Carlo beyond a million samples had no effect on the statistics of the estimated quantities for the number of significant digits reported. The Monte Carlo simulations probably overestimated the variance of relevant ratios such as  $w/L$  and  $t/L$  in comparison to hominin feet, because we use independent variation of all dimensions and do not incorporate covariation that may exist. Such inflation of variance because of an assumption of independence of variables is evident when comparing primary measurements to Monte Carlo estimation of  $\hat{c}$  for humans (Extended Data Table 2).

## Morphometrics of feet of extant species

**Humans.** Human morphometrics were obtained from 12 individuals (6 cadaveric, 6 human volunteers) using radiographic computed tomography (CT X-ray imaging) and software-based segmentation and three-dimensional model reconstruction. These feet were all evaluated by a clinical radiologist and identified as non-pathological. The collection, analyses and reporting of data from live human subjects were approved by the Yale IRB. Details on the subjects and CT data-processing methods are provided in Supplementary Information 5.1.

We measured the lever length  $L$  following the standard definition as the distance from the posterior end of the calcaneus to the anterior

end of the distal head of the third metatarsal. The width  $w$  is measured at the tarsometatarsal joint, as the mediolateral separation of the most medial aspect of the distal articular surface of the medial cuneiform to the most lateral aspect of the distal articular surface of the cuboid. The thickness  $t$  is defined as the dorso-plantar thickness of the proximal head of the third metatarsal, or the average of the second and fourth, when the third metatarsal data are unavailable. The curvature  $c$  is based on the torsion  $\theta_{\text{MT4}}$  of the fourth metatarsal, which was measured using the shape of the articular surface using established protocols<sup>28</sup>.

## Non-human primates

Published data were used for morphometrics analysis of non-human primates: *P. troglodytes* ( $n = 106$ )<sup>28–30,32–34</sup>, *G. gorilla* ( $n = 59$ )<sup>28–30,32–34</sup>, *C. aethiops* ( $n = 56$ )<sup>32,35</sup> and *M. nemestrina* ( $n = 44$ )<sup>32,36,37</sup>.

Published data are sparse and not all required measurements were available for a single sample in the published literature for *C. aethiops* and *M. nemestrina*. Therefore, we added data from specimens that were most similar in their lever length  $L$  to the mean value reported in the literature. We carried out these measurements using software-based photogrammetry<sup>38</sup> of high-resolution images and cross-verified with measurements using a digital caliper (0.01 mm resolution). The *C. aethiops* foot is from the Yale Biological Anthropology Laboratory (YBL.3032a) and the *M. nemestrina* specimen from the Yale Peabody Museum (YPM MAM 9621).

The mean and s.d. of the lever length  $L$  were estimated from published data for chimpanzee<sup>32–34</sup>, gorilla<sup>32,34</sup>, *C. aethiops*<sup>32,35</sup> and *M. nemestrina*<sup>32,36,39</sup>. Mean  $w$  is estimated from reported  $w/L$  or dorsal skeletal views for chimpanzees and gorillas<sup>32,33</sup>, and primary measurements for *C. aethiops* and *M. nemestrina*. To estimate the s.d. of  $w$ , we used reported variability in the medio-lateral width of the proximal metatarsal heads for all species<sup>28–30</sup> to estimate the coefficient of variation (s.d./mean), and applied that to  $w$ . The mean and s.d. of  $t$  were all obtained from published values<sup>29,30</sup> and confirmed with primary measurements for available specimens. Torsion of the fourth metatarsal  $\theta_{\text{MT4}}$  is used to estimate the transverse curvature and published values were used for all non-human species included in this study<sup>26,28–30</sup>. For species for which the feet are regarded as flat, we used the same metatarsal torsion values as *P. troglodytes*.

## Fossil feet

We used photogrammetry<sup>38</sup> on published images of fossil feet (Fig. 4d), as well as data tables that accompanied the publication of these fossil data to estimate the necessary dimensions and ratios<sup>26–30</sup>.

Among the fossil feet, all except the foot of *H. naledi*<sup>26</sup> were incomplete in some regard. For those incomplete feet, an extant species was selected as a template by taking into consideration published analyses of other postcranial and cranial elements. On the basis of this information, *H. sapiens* was chosen as the template for *H. erectus* (Dmanisi)<sup>28</sup> and *H. habilis* (Olduvai hominin)<sup>27</sup> and *G. gorilla* was chosen as the template for *A. afarensis* (AL 333)<sup>30</sup> and the unknown hominin foot found in Burtele<sup>29</sup>. For example, the sole fourth metatarsal of *A. afarensis* does not permit the direct estimation of  $w$ . However, only the ratio  $w/L$  is necessary for the analyses, and the ratio of gorilla is used for the Monte Carlo analysis of the fossil. The metatarsal, however, provides a direct measurement of  $t$ , but not of  $L$ . Therefore, to estimate the ratio  $t/L$ , we incorporate the measured thickness  $t$  and the gorilla's ratio  $t_g/L_g$  by using the formula

$$\frac{t}{L} = \frac{t}{\langle t_g \rangle} \frac{t_g}{L_g} \quad (4)$$

in which  $\langle t_g \rangle$  is the mean  $t$  of gorilla. This template-based estimation therefore incorporates direct measurements where available, without assuming that the fossil exactly resembles the extant template.

## Curvature of hominin feet from metatarsal torsion

Following standard practice in the literature<sup>28,30</sup>, we use the torsion of the fourth metatarsal ( $\theta_{MT4}$ ) to estimate TTA curvature. This measure also facilitates the estimation of TTA curvature using partial or disarticulated fossils. When the proximal metatarsal heads form a transverse arch and the distal metatarsal heads rest on the ground, the lateral metatarsals increasingly acquire torsion about their long axis (Fig. 4b and Extended Data Fig. 6b, c). We compared the torsion-based estimate of curvature versus using the external geometry of the dorsal surface of the skeleton and found good correspondence (Extended Data Fig. 6d and Supplementary Information 5.1). The torsion  $\theta_{MT4}$  arises from the curvature  $c$  over the width  $w$  of the tarso-metatarsal articulation and therefore the curvature is approximated by  $c = \theta_{MT4}/w$ . Using equation (1), the torsion-based estimate of the normalized curvature parameter for the TTA is

$$\hat{c} = \frac{\theta_{MT4}}{(w/L)(t/L)} \quad (5)$$

## Reporting summary

Further information on research design is available in the Nature Research Reporting Summary linked to this paper.

## Data availability

The data supporting the findings of this study are available within the paper and its Supplementary Information.

32. Schultz, A. H. Relations between the lengths of the main parts of the foot skeleton in primates. *Folia Primatol.* **1**, 150–171 (1963).
33. Gomberg, D. N. *Form and Function of The Hominoid Foot*. PhD thesis, Univ. Massachusetts, Amherst (1981).

34. Wang, W. J. & Crompton, R. H. Analysis of the human and ape foot during bipedal standing with implications for the evolution of the foot. *J. Biomech.* **37**, 1831–1836 (2004).
35. Anapol, F., Turner, T. R., Mott, C. S. & Jolly, C. J. Comparative postcranial body shape and locomotion in *Chlorocebus aethiops* and *Cercopithecus mitis*. *Am. J. Phys. Anthropol.* **127**, 231–239 (2005).
36. Sirianni, J. E., Swindler, D. R. & Tarrant, L. H. Somatometry of newborn *Macaca nemestrina*. *Folia Primatol.* **24**, 16–23 (1975).
37. Rodman, P. Skeletal differentiation of *Macaca fascicularis* and *Macaca nemestrina* in relation to arboreal and terrestrial quadrupedalism. *Am. J. Phys. Anthropol.* **51**, 51–62 (1979).
38. Schindelin, J. et al. Fiji: an open-source platform for biological-image analysis. *Nat. Methods* **9**, 676–682 (2012).
39. Hamada, Y. Standard growth patterns and variations in growth patterns of the Japanese monkeys (*Macaca fuscata*) based on an analysis by the spline function method. *Anthropol. Sci.* **102**, 57–76 (1994).
40. Hessman, F. V. Figure Calibration: a plug-in for ImageJ. [http://www.astro.physik.uni-goettingen.de/~hessman/ImageJ/Figure\\_Calibration](http://www.astro.physik.uni-goettingen.de/~hessman/ImageJ/Figure_Calibration) (2009).

**Acknowledgements** We thank D. Lieberman for discussions on the manuscript and S. Piazza for constructive contributions. Access to skeletal specimens was provided by G. Aronsen, K. Zyskowski, E. Sargis, Yale Biological Anthropology Laboratories and the Yale Peabody Museum. K. J. Meacham III provided experimental support. S. James helped with figures. Funding support came from the Human Frontier Science Program.

**Author contributions** M.V., M.M.B. and S.M. conceived the study; A.Y. and M.V. designed the foot mimics and A.Y. performed the experiments; C.M.E., A.Y. and M.V. designed, collected and analysed the data from the cadaveric experiments in consultation with S.M.T.; A.Y., C.M.E. and M.V. collected and analysed the morphometric data from cadaveric and living human feet in consultation with A.H.H.; M.A.D. and S.M. performed the mathematical modelling in consultation with M.V.; D.K.S. and M.M.B. performed the shell experiments in consultation with M.V.; M.V. planned and wrote the paper; M.V. planned and prepared the figures and tables; M.V., A.Y., S.M., M.A.D. and M.M.B. wrote the Supplementary Information; and all authors contributed to editing the paper.

**Competing interests** The authors declare no competing interests.

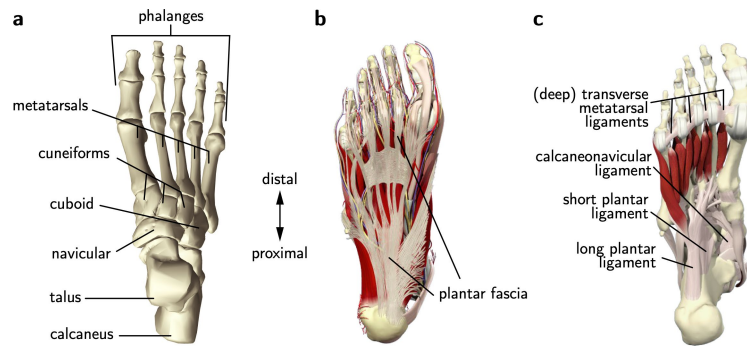
## Additional information

**Supplementary information** is available for this paper at <https://doi.org/10.1038/s41586-020-2053-y>.

**Correspondence and requests for materials** should be addressed to M.V., M.M.B. or S.M.

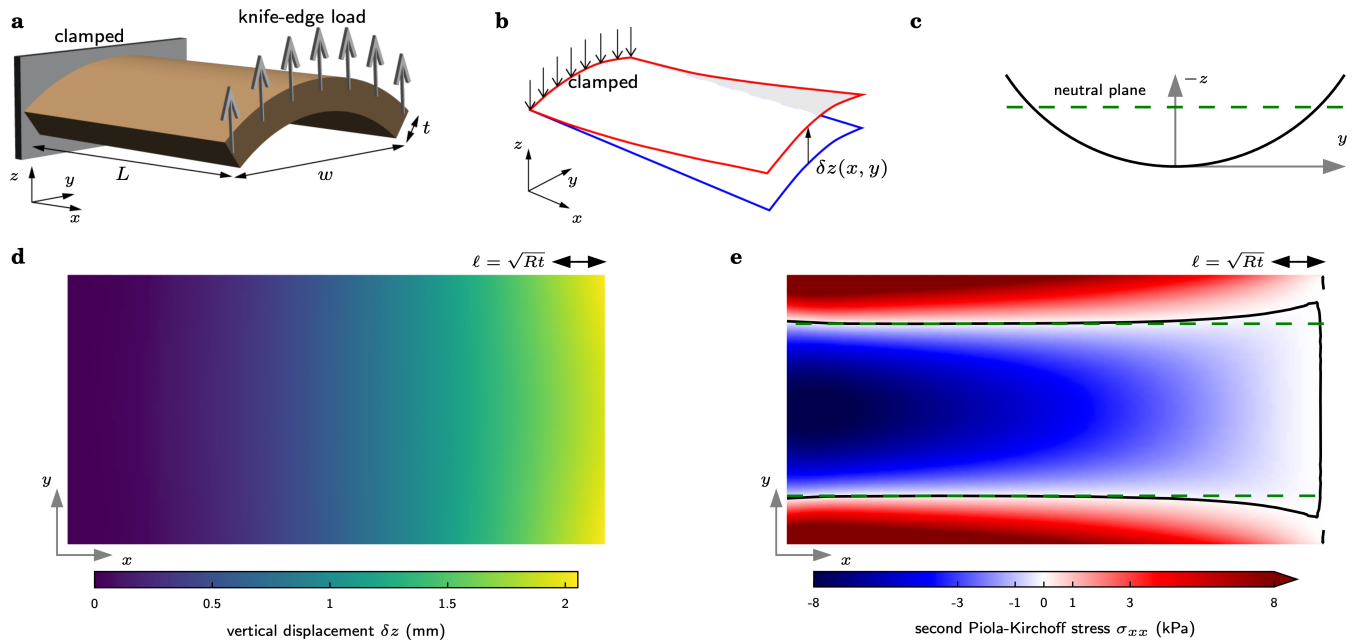
**Peer review information** Nature thanks Stephen Piazza and the other, anonymous, reviewer(s) for their contribution to the peer review of this work.

**Reprints and permissions information** is available at <http://www.nature.com/reprints>.



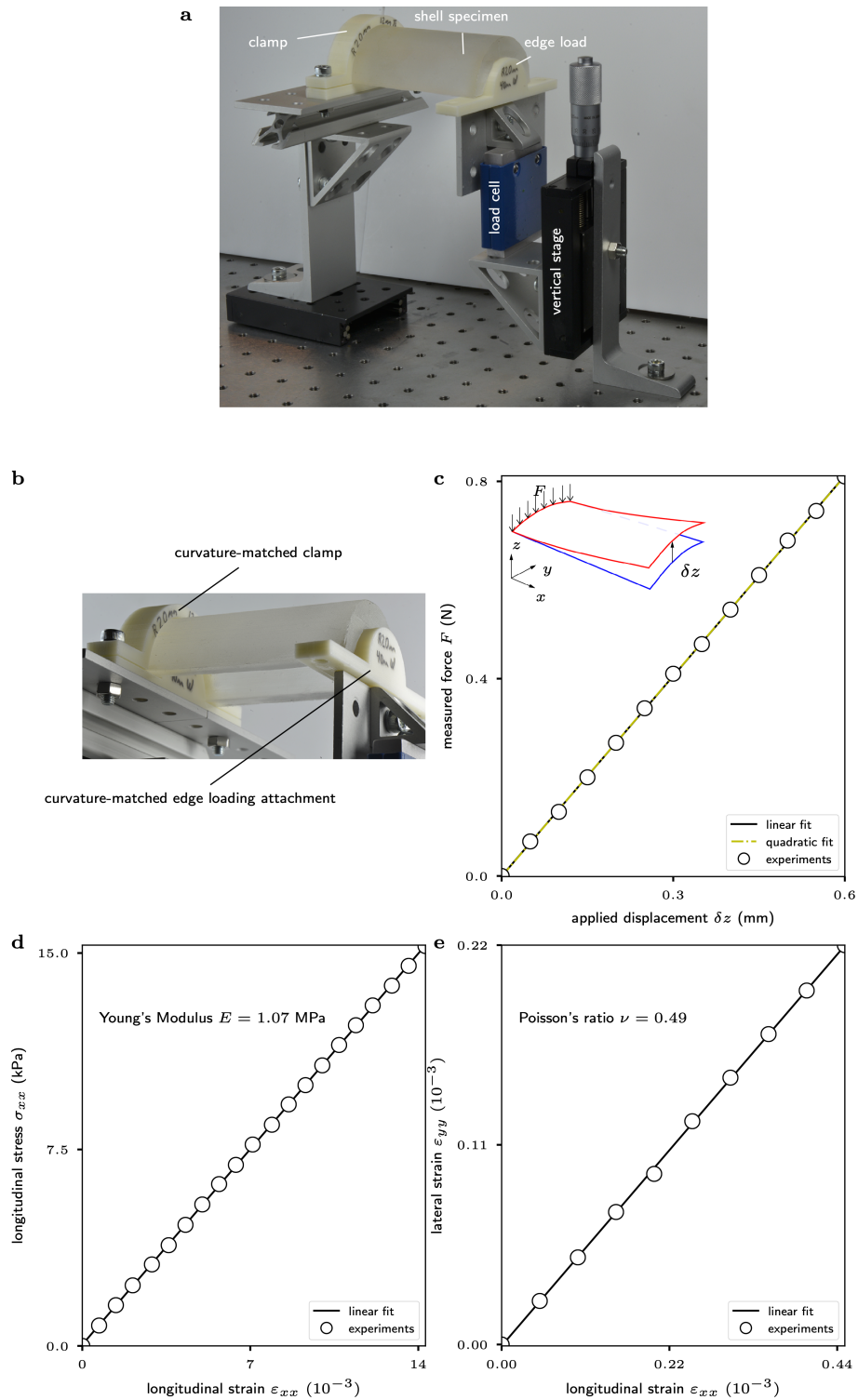
**Extended Data Fig. 1 | Illustrated anatomy of the foot.** **a**, Identification of the bones of the foot that are referred to in the main text. The cuneiforms, cuboid and the navicular are collectively referred to as the tarsal bones. **b**, The plantar fascia, a tough elastic band, extends from the calcaneus to the distal end of the phalanges. The fascia split and rejoin at multiple locations. **c**, The long plantar,

short plantar and calcaneonavicular ligaments are located in the midfoot and are primarily longitudinally oriented. The deep and superficial transverse metatarsal ligaments are examples of stiff, transversally oriented elastic tissues between the metatarsals. Anatomical images are from Primal Pictures.



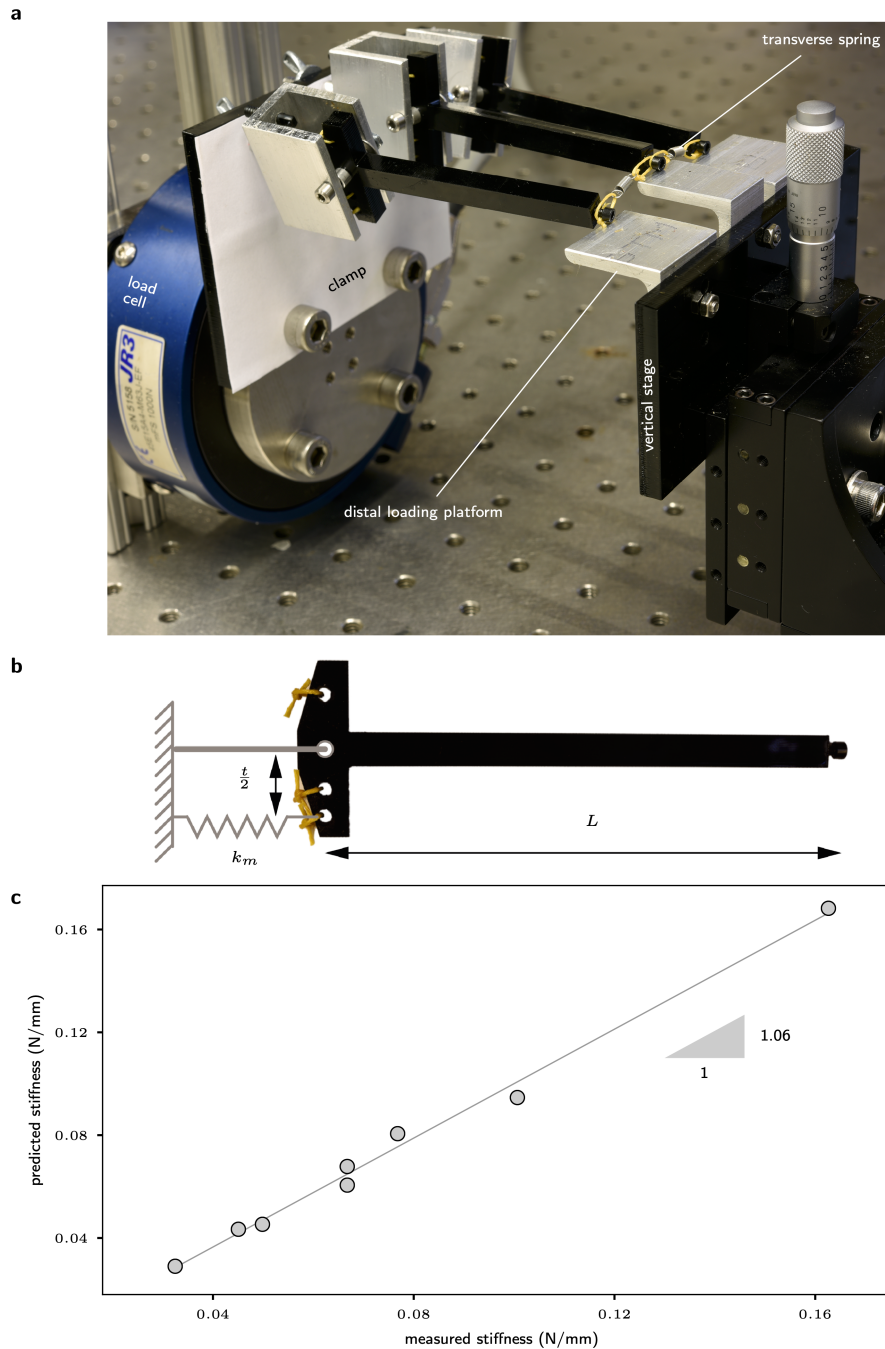
**Extended Data Fig. 2 | Mathematical and computational analysis of continuum elastic shells.** **a**, The shell is clamped at one end and loaded with a knife edge at the other. It is of length  $L$ , width  $w$ , thickness  $t$  and has radius of curvature  $R$  (curvature  $c=1/R$ ). **b**, The free end displaces by a height  $\delta z$  on loading and reaction forces at the clamped end resist deformation. **c**, A cross-sectional view of the shell shows the location of the neutral plane, if the shell were to act as an elastic beam. **d**, Out-of-plane ( $z$ -axis) displacement profile for one numerical simulation of a shell ( $L=0.1$  m,  $w=0.05$  m,  $t=0.003$  m,

$R=0.03$  m). Most of the displacement happens close to the loaded edge, unlike an elastic beam. **e**, The stress component  $\sigma_{xx}$  is shown as a colour map of the undeformed shell. In an elastic beam, the intersection of the neutral plane with the shell (**c**) would exactly match the locations of zero stress. Because of curvature-induced in-plane stretching, the zero-stress curve differs from the neutral plane predictions in the vicinity of the loaded edge and—to a lesser extent—near the clamped boundary.



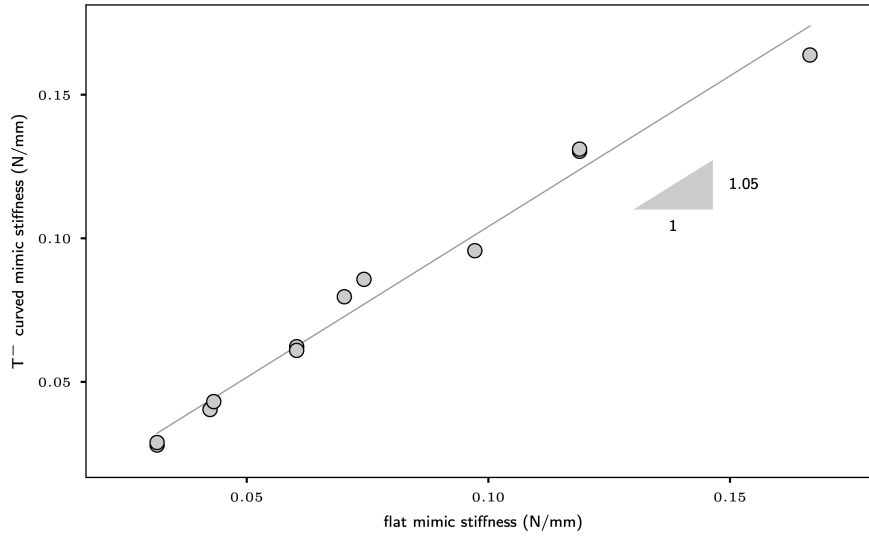
**Extended Data Fig. 3 | Experimental characterization of arched shells. a,** The experimental set-up used in stiffness measurements. **b,** A magnification of the shell from underneath shows how a curvature-matched edge-loading attachment was used to mimic a theoretical knife edge. A curvature-matched clamp was fixed and glued to the other end of the shell. **c,** Representative data

that show the linearity of the force–displacement data. The best-fit quadratic is indistinguishable from the linear fit to within sensor resolution. **d, e,** The Young's modulus (**d**) and Poisson's ratio (**e**) of the PDMS material used to fabricate the shells were estimated from simultaneous stress and strain measurements during an extension test of a rectangular PDMS block.

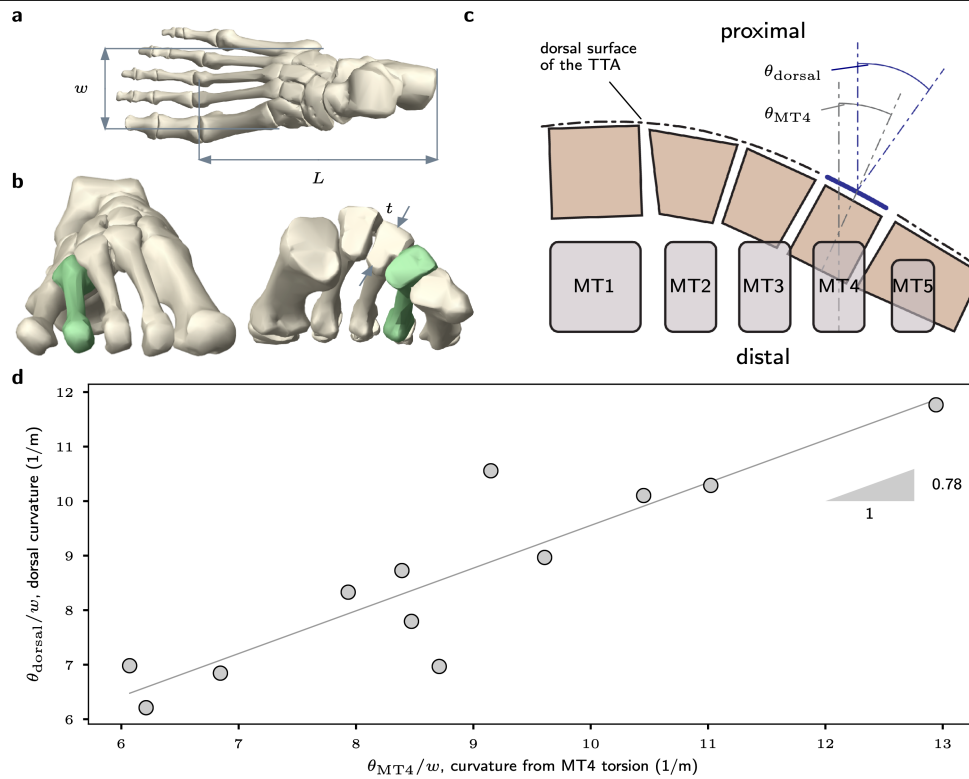


**Extended Data Fig. 4 | Design and characterization of discrete mechanical foot mimics. a,** Experimental arrangement for load–displacement measurements. The distal loading platforms for the three metatarsals are staggered in height so that all three metatarsals are loaded vertically despite the transverse curvature. In hominin feet, this is accomplished by the metatarsal torsion. **b,** Side view of a single metatarsal showing length  $L$  and thickness  $t$  of the foot mimics. The effect of thickness is to provide a moment arm for the longitudinal spring and thus affect the rotational stiffness of the

hinge. **c,** Mimics with three different thicknesses were fabricated and the thickness was estimated using load–displacement measurements on curvature-free flat mimics. The accuracy of the estimated thickness values are evaluated by plotting the predicted stiffness based on the thickness estimates against the measured stiffness. Details of the thickness estimation technique and statistics of the stiffness–stiffness correlation are provided in Supplementary Information 4.4.



**Extended Data Fig. 5 | Effect of cutting the transverse springs in mechanical foot mimics.** Stiffness of transversally curved foot mimics lacking the transverse inter-metatarsal springs ( $T^-$ ) is strongly correlated with the stiffness of flat mimics with intact transverse inter-metatarsal springs.



**Extended Data Fig. 6 | Transverse curvature of hominin feet.** **a**, Definitions of length  $L$  and width  $w$ . **b**, Definition of the thickness  $t$ . The fourth metatarsal is highlighted in green. The distal heads of the metatarsals rest flat on the ground and the proximal heads are raised away from the ground to different degrees because of the TTA. **c**, Schematic showing the accrual of torsion on the lateral metatarsals about their long axis. The curvature of the TTA was estimated using

the torsion of the fourth metatarsal  $\theta_{\text{MT4}}$ . In addition, the average curvature was also estimated using the angle of the normal to the dorsal surface of the fourth metatarsal  $\theta_{\text{dorsal}}$ , as measured in the midfoot (Supplementary equation (5.3)). **d**, Linear regression of the two methods to estimate TTA curvature. Details of the curvature estimation procedure and statistical results of the regression are provided in Supplementary Information 5.1.

**Extended Data Table 1 | The estimated work during foot deformation**

Species	Foot condition	Variable	Value
Cadaveric data collected for this study			
<i>Homo sapiens</i> , sample 1	intact	$W_h$	5.5 J
	–transverse tissue	$W_{T-}$ $(W_h - W_{T-})/W_h$	3.1 J 44%
<i>Homo sapiens</i> , sample 2	intact	$W_h$	7.4 J
	–transverse tissue	$W_{T-}$ $(W_h - W_{T-})/W_h$	3.4 J 54%
Previously published <sup>9,18</sup> cadaveric data			
<i>Homo sapiens</i>	intact	$W_h$	10.1 J
	–plantar fascia	$W_{h,pf-}$ $(W_h - W_{h,pf-})/W_h$	7.8 J 23%
	–long plantar ligament	$W_{h,lp-}$ $(W_{h,pf-} - W_{h,lp-})/W_h$	4.6 J 32%
	–short plantar ligament	$W_{h,sp-}$ $(W_{h,lp-} - W_{h,sp-})/W_h$	2.1 J 25%
	–calcaneonavicular ligament	$W_{h,cn-}$ $(W_{h,sp-} - W_{h,cn-})/W_h$	1.2 J 9%
	<i>Macaca nemestrina</i>	intact	$W_m$
plantar fascia removed		$W_{m,pf-}$ $(W_m - W_{m,pf-})/W_m$	5.0 J 2%
–long plantar ligament		$W_{m,lp-}$ $(W_{m,pf-} - W_{m,lp-})/W_m$	3.1 J 37%
–calcaneonavicular ligament		$W_{m,cn-}$ $(W_{m,lp-} - W_{m,cn-})/W_m$	2.4 J 14%
<i>Chlorocebus aethiops</i>	intact	$W_c$	3.9 J

Data are obtained from cadaveric tests and from published load versus displacement data for humans<sup>9</sup>, *C. aethiops* and *M. nemestrina*<sup>18</sup>. In addition to the foot deformation work of the intact human foot ( $W_h$ ), the cadaveric experiments performed in this study included the transection of the transverse inter-metatarsal elastic tissues, shown as  $W_{T-}$ . The peak displacements in the tests were 12 mm and 13 mm for samples 1 and 2, respectively. The published data for the three species include intact feet ( $W_h$ ,  $W_m$  and  $W_c$ ) and feet with transection of the plantar fascia ( $W_{h,pf-}$ ), the long plantar ligament ( $W_{h,lp-}$ ), the short plantar ligament ( $W_{h,sp-}$ ) and the calcaneonavicular ligament ( $W_{h,cn-}$ ). These estimates were obtained by digitizing the published plots<sup>9,18</sup> of load versus displacement and measuring the area under the curve as the foot was loaded<sup>38,40</sup>. The contribution of each of the transected tissues are represented as the ratio of the decrease in work after transection to the intact stiffness of the same foot. The previously published transections<sup>9,18</sup> were performed in the same sequence as listed in this table. Raw data are available for the two cadaveric specimens as Supplementary Information.

**Extended Data Table 2 | Foot morphometrics for extant species**

Species	$L$ (mm)		$w$ (mm)		$t$ (mm)		$\theta_{MT4}$ (deg)		$\hat{c}$	
	mean	SD	mean	SD	mean	SD	mean	SD	mean	SD
<i>Homo sapiens</i> <sup>a</sup>	177	16.9	50.7	4.0	16.1	1.6	25.0	4.6	16.9	2.7
<i>Homo sapiens</i> <sup>b</sup>	200	14.0	60.0	5.4	18.0	1.6	23.6	7.1	15.6	5.6
<i>Chlorocebus aethiops</i>	85.0	4.3	24.0	1.2	9.0	0.45	0	2.5	0.0	1.5
<i>Macaca nemestrina</i>	100	6.0	35.0	2.1	10.0	0.6	0	2.5	0.0	1.3
<i>Pan troglodytes</i>	130	13.0	52.0	5.2	13.0	1.3	0	2.5	0.0	1.2
<i>Gorilla gorilla</i>	176	17.6	72.5	7.3	16.0	1.6	2.2	1.5	1.1	0.8

<sup>a</sup>Primary data collected by us from 12 samples.

<sup>b</sup>Bootstrapped Monte Carlo analysis using published data.

Metrics were obtained from primary data for humans and Monte Carlo estimates for all species. For the Monte Carlo estimation, the dimensions are modelled as Gaussian random variables. Mean  $\pm$  s.d. values were obtained from values reported in the literature (see 'Morphometrics of feet of extant species' in the Methods for details). Although the primary data were smaller feet than the published data, the ratios  $w/L$  and  $t/L$  were almost equal. The morphometric variables are the lever length of the foot  $L$ , width of the tarso-metatarsal articular region  $w$ , dorso-plantar thickness of the third metatarsal  $t$  and torsion of the fourth metatarsal  $\theta_{MT4}$ . From these, the normalized curvature parameter  $\hat{c}$  was estimated.

# Article

**Extended Data Table 3 | Fossil morphometric data**

Species	Specimen	$\theta_{MT4}$ (deg)	$L$ (mm)	$w$ (mm)	$t$ (mm)	$w/L$	$t/L$
<i>H. naledi</i>	UW 101-1456	38.0	137.0	38.0	16.0	0.277	0.117
<i>H. erectus</i>	D2669, D4165	28.0, 29.0	–	–	17.0	$\frac{w_h}{L_h}$	$\frac{t}{\langle t_h \rangle} \frac{t_h}{L_h}$
<i>H. habilis</i>	OH 8	25.0	112	44.0	–	0.393	$\frac{t_h}{L_h}$
Burtele	BRT VP2/73	26.5	–	–	13.3	$\frac{w_g}{L_g}$	$\frac{t}{\langle t_g \rangle} \frac{t_g}{L_g}$
<i>A. afarensis</i>	AL 333-160	17.0	–	–	17.1	$\frac{w_g}{L_g}$	$\frac{t}{\langle t_g \rangle} \frac{t_g}{L_g}$

Values of  $L$ ,  $w$ ,  $t$  and  $\theta_{MT4}$  used in estimating the normalized curvature  $\hat{c}$  of fossil samples. Variable names with a subscript h refer to human values (for example,  $t_h$ ), subscript p to chimpanzee (for example,  $w_p$ ) and subscript g to gorilla (for example,  $L_g$ ). These values are represented by normal distributions as shown in Extended Data Table 2. Variables in angled brackets, such as  $\langle t_h \rangle$ , refer to the mean value shown in Extended Data Table 2. See Methods for details of source materials.

## Reporting Summary

Nature Research wishes to improve the reproducibility of the work that we publish. This form provides structure for consistency and transparency in reporting. For further information on Nature Research policies, see [Authors & Referees](#) and the [Editorial Policy Checklist](#).

### Statistics

For all statistical analyses, confirm that the following items are present in the figure legend, table legend, main text, or Methods section.

n/a Confirmed

- The exact sample size ( $n$ ) for each experimental group/condition, given as a discrete number and unit of measurement
- A statement on whether measurements were taken from distinct samples or whether the same sample was measured repeatedly
- The statistical test(s) used AND whether they are one- or two-sided  
*Only common tests should be described solely by name; describe more complex techniques in the Methods section.*
- A description of all covariates tested
- A description of any assumptions or corrections, such as tests of normality and adjustment for multiple comparisons
- A full description of the statistical parameters including central tendency (e.g. means) or other basic estimates (e.g. regression coefficient) AND variation (e.g. standard deviation) or associated estimates of uncertainty (e.g. confidence intervals)
- For null hypothesis testing, the test statistic (e.g.  $F$ ,  $t$ ,  $r$ ) with confidence intervals, effect sizes, degrees of freedom and  $P$  value noted  
*Give  $P$  values as exact values whenever suitable.*
- For Bayesian analysis, information on the choice of priors and Markov chain Monte Carlo settings
- For hierarchical and complex designs, identification of the appropriate level for tests and full reporting of outcomes
- Estimates of effect sizes (e.g. Cohen's  $d$ , Pearson's  $r$ ), indicating how they were calculated

*Our web collection on [statistics for biologists](#) contains articles on many of the points above.*

### Software and code

Policy information about [availability of computer code](#)

Data collection

Continuum shell experiments: Labview (National Instruments)  
Cadaveric experiments: FastTrack 8800 (Instron, MA, USA)  
Foot mimics: Vicon Nexus 1.8 (Oxford, UK)

Data analysis

CT reconstruction and morphometrics:  
\* ITK-SNAP 3.6.0, Yushkevich, P. A. et al., Neuroimage 31, 1116-1128 (2006).  
\* 3DSlicer 4.8.1, Fedorov, A. et al., Magn Reson Imaging 30, 1323-41 (2012) [www.slicer.org](http://www.slicer.org).  
\* FIJI 1.52i: Schindelin, J. et al. Fiji: an open-source platform for biological-image analysis. Nature Methods 9, 676-82 (2012)  
Elasticity simulation using COMSOL Multiphysics v5.1 (COMSOL AB, Stockholm, Sweden).  
Data analyses for foot mimics: MATLAB R2019a (Mathworks, USA)  
Data analyses of morphometric data: Python v3.7.5, Numpy v1.17.4

For manuscripts utilizing custom algorithms or software that are central to the research but not yet described in published literature, software must be made available to editors/reviewers. We strongly encourage code deposition in a community repository (e.g. GitHub). See the Nature Research [guidelines for submitting code & software](#) for further information.

### Data

Policy information about [availability of data](#)

All manuscripts must include a [data availability statement](#). This statement should provide the following information, where applicable:

- Accession codes, unique identifiers, or web links for publicly available datasets
- A list of figures that have associated raw data
- A description of any restrictions on data availability

The authors declare that the data supporting the findings of this study are available within the paper and its supplementary information files.

## Field-specific reporting

Please select the one below that is the best fit for your research. If you are not sure, read the appropriate sections before making your selection.

Life sciences     Behavioural & social sciences     Ecological, evolutionary & environmental sciences

For a reference copy of the document with all sections, see [nature.com/documents/nr-reporting-summary-flat.pdf](https://www.nature.com/documents/nr-reporting-summary-flat.pdf)

## Life sciences study design

All studies must disclose on these points even when the disclosure is negative.

Sample size	This study analyses previously published (and fully cited) data on foot stiffness and geometry, the details of which are part of the original publication. Other data were generated from images of unique fossil specimens or computer simulations, where sample size is not a consideration. The mechanical foot-mimics were chosen to span the relevant parameter range, which determined the sample size. Cadaveric feet were limited by availability of healthy feet and used a small sample size (n=2) similar to prevalent practice in the field. In this case, the small cadaveric sample size is justified because we directly tested a mechanism through dissections and not used the data for performing statistical estimations. Finally, we used 12 human feet for morphometrics and the sample size was determined by sample sizes that are standard practice in the field.
Data exclusions	No data were excluded.
Replication	To aid reproducibility, this study uses Monte Carlo simulations as part of a bootstrap approach to incorporate anatomical variability in the estimated quantities. Mean and standard deviations for random variables that enter the Monte Carlo are based on published (and cited) values. Furthermore, for the morphometric measurements, multiple authors independently carried out the data analyses. These efforts at replication were successful because the Monte Carlo converged, i.e. increasing number of simulations did not change the reported statistics, and the repetition of morphometric measurements by different authors yielded the consistent results.
Randomization	This study uses previously published data or unique specimen such as fossils, and therefore randomized allocation to groups is not a consideration. For the cadaveric experiments, the intact foot tests had to necessarily precede the intervention of cutting the inter-metatarsal tissues. Therefore, randomization is not possible. The measurements were automated and did not involve subjective processing and therefore blinding is not relevant.
Blinding	Blinding does not apply to this study for same reasons as randomization.

## Reporting for specific materials, systems and methods

We require information from authors about some types of materials, experimental systems and methods used in many studies. Here, indicate whether each material, system or method listed is relevant to your study. If you are not sure if a list item applies to your research, read the appropriate section before selecting a response.

### Materials & experimental systems

n/a	Involvement in the study
<input checked="" type="checkbox"/>	<input type="checkbox"/> Antibodies
<input checked="" type="checkbox"/>	<input type="checkbox"/> Eukaryotic cell lines
<input type="checkbox"/>	<input checked="" type="checkbox"/> Palaeontology
<input checked="" type="checkbox"/>	<input type="checkbox"/> Animals and other organisms
<input type="checkbox"/>	<input checked="" type="checkbox"/> Human research participants
<input checked="" type="checkbox"/>	<input type="checkbox"/> Clinical data

### Methods

n/a	Involvement in the study
<input checked="" type="checkbox"/>	<input type="checkbox"/> ChIP-seq
<input checked="" type="checkbox"/>	<input type="checkbox"/> Flow cytometry
<input checked="" type="checkbox"/>	<input type="checkbox"/> MRI-based neuroimaging

## Palaeontology

Specimen provenance	All paleontological data in this study are from past publications that report on the specimen. Therefore, provenance determination is part of the past studies, which are cited in the manuscript as needed.
Specimen deposition	The data on the specimens were all from publicly available publications, and their complete citation information is provided in the manuscript.
Dating methods	No new dates are provided.
<input type="checkbox"/>	Tick this box to confirm that the raw and calibrated dates are available in the paper or in Supplementary Information.

## Human research participants

Policy information about [studies involving human research participants](#)

Population characteristics	<p>The human participants were comprised of 5 females and 1 male of age 35years to 68years, body height 150cm to 183cm and body mass 45kg to 97kg. The medical records and scans of these subjects were examined by a clinical radiologist and certified to be free of known diseases or deformities. The cadaveric samples were from 2 female and 4 male donors of age 55 years to 74 years, body height 160 cm to 185 cm and body mass 61 kg to 110 kg, which were amputated at the mid-tibia. The samples are obtained from consenting donors with no known foot diseases or deformities.</p>
Recruitment	<p>The live human data are from pre-existing CT scans of feet from patients that visited the Yale New Haven Hospital for foot diagnostics unrelated to this study. Because these subjects are from patients who had their feet scanned for clinical reasons, there is the potential for bias that they belong to a subset of the population that manifests pathologies or other changes to their feet. However, we consulted a clinical radiologist who examined a large cohort of patients and aided in the selection of only those who did not manifest any diseases or deformities. Furthermore, the clinician augmented the inspection of the radiological data with the notations on the patient's record to ensure that no cause for exclusion existed.</p> <p>The cadaveric samples were from Medcure, a body donation program that is accredited by the American Association of Tissue Banks (AATB). Medcure supports medical science by providing access to body donors for researchers. In seeking foot specimens from body donors via Medcure, we used the following criteria: no foot or leg injuries or surgeries, aged between 20 and 75, no history of diabetes, and paired feet. Importantly, the specimens were not from amputees, rather from deceased individuals who died of causes unrelated to their feet. Therefore, the specimen are likely representative of healthy feet.</p>
Ethics oversight	<p>The Yale University IRB approved the use of CT scans collected from patients. Because the data were de-identified of all patient information, the research was granted an exemption from IRB review under federal regulation 45 CFR 46.101(b)(4). This part of the federal regulations covers research involving the collection or study of existing data, documents, records, pathological specimens, or diagnostic specimens, if these sources are publicly available or if the information is recorded by the investigator in such a manner that subjects cannot be identified, directly or through identifiers linked to the subjects.</p> <p>For the cadaveric specimens, there was no IRB approval needed since a) the subjects were not living and b) the samples were deidentified and obtained from consenting donors.</p> <p>Record of consent comes from the MedCure contract (Form F-152B):          "Legal consent is obtained from all donors in accordance with the Uniform Anatomical Gift Act (UAGA) and all state and federal laws and regulations. This consent is obtained prior to specimen procurement and distribution. MEDCURE abides by Title 45, Part 46 of the U.S. Code of Federal Regulations protecting the identity of the donor."</p>

Note that full information on the approval of the study protocol must also be provided in the manuscript.